Is the Amik Basin (SE Turkey) a triple-junction area? Analyses of SPOT XS imagery and seismicity

S. OVER†, K. Ş. KAVAK‡, O. BELLIER§ and S. ÖZDEN‡
†Cumhuriyet Universitesi Jeofizik Mühendisliği, 58140-Sivas, Turkey;
e-mail: over@cumhuriyet.edu.tr
‡Cumhuriyet Universitesi Jeoloji Mühendisliği, 58140-Sivas, Turkey
§CEREGE-UMR CNRS 6635- Université Aix Marseille III, BP 80, Europôle Mediterranéen de l'rbois-13545 Aix en Provence Cedex 4, France

Abstract. In the eastern Mediterranean, plate motions occur between the Arabia/Anatolia, Africa/Arabia and Anatolia/Africa boundaries along the Amanos Fault, the Dead Sea Fault and the Cyprus Arc, and the extension of the latter on land. Detailed enhancement and classification procedures applied to SPOT XS imagery of the Hatay region, and centred on the Quaternary Amik Basin, have revealed a prominent NE–SW-trending tectonic lineament. Recent seismicity suggests that this NE–SW-trending lineament dies out in the Quaternary Amik Basin in the east and continues to the Cyprus Arc to the south-west. Structural lineament extensions derived from SPOT XS imagery using linear edge enhancement and unsupervised classification methods and the distribution of seismicity in the Hatay region show that this region has been affected by the East Anatolian Fault Zone, the Dead Sea Fault Zone and the Cyprus–Antakya Transform fault. These fault associations accommodate northerly movement of the African and Arabian plates toward the Eurasian plate. The Amik Basin appears to have been formed by interaction among the Amanos Fault interpreted here as a continuation of the East Anatolian Fault the left-lateral Dead Sea Fault, and the left-lateral Cyprus–Antakya transform fault. Active faults belonging to the aforementioned structural zones meet one another to form a triple junction at the Amik Basin near Antakya.

1. Introduction

The Hatay region is located at the northastern corner of the eastern Mediterranean region in southeastern Turkey and lies in an intersection domain between the East Anatolian Fault Zone (EAFZ), the Dead Sea Fault Zone (DSFZ), and the Cyprus Arc and its on-land extension (figure 1). This domain accommodates the relative motions of Arabia/Anatolia, Africa/Arabia, and Anatolia/Africa (McKenzie 1972, 1978; Le Pichon and Angelier 1979, Şengör 1979, Jackson and McKenzie 1984, Dewey *et al.* 1986, Westaway 1994, Westaway and Arger 1996).

This study is mainly focused on analysis of the extension of the Cyprus Arc to the vicinity of Antakya in south-eastern Turkey (figure 1), which will be referred to here as the Cyprus–Antakya Transform (CAT). To date, this segment has been much less investigated than the two other major components of the triple-junction region (i.e. the EAFZ and DSFZ).

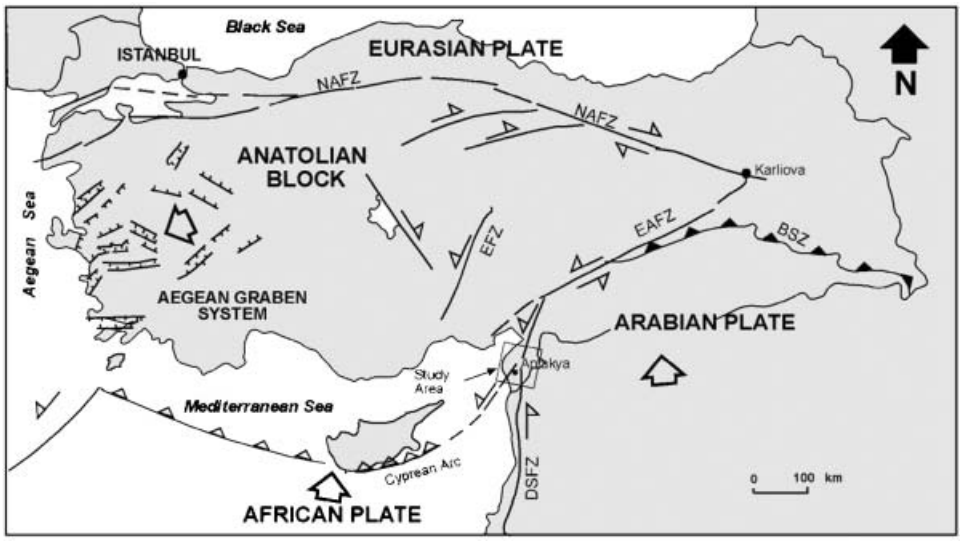


Figure 1. Sketch map of the eastern Mediterranean tectonic framework (modified after Şengor 1979, Gürsoy *et al.* 1998, Över *et al.* 2002).

The goal of the present study was to identify the image-processing opportunities for geologic/tectonic applications, especially designed for SPOT XS (K/J No. 118/277) imagery data of the Hatay region, centred on the Amik Basin of Quaternary age. In this study we have carried out a tectonic analysis of the major structures and their relationships based on a lineament analysis of SPOT XS images, and have supported our study with seismotectonic analysis. Finally, we discuss the location of the Antakya triple-junction area (ATJ) in the context of the Quaternary Amik Basin.

2. Tectonic setting of the Hatay region

Active deformation in the eastern Mediterranean region, particularly in Anatolia, has occurred as a result of continental collision between the Afro-Arabian and Eurasian plates since the Late Miocene, following closure of the Neotethys oceanic basin at a collisional boundary corresponding to the Bitlis suture (Şengör *et al.* 1985).

2.1. *Plate motions and fault systems*

The study area, shown in figure 1, lies in an intersection domain among three active belts: the southern end of the left-lateral East Anatolian Fault (EAF), the northern end of the left-lateral Dead Sea Fault (DSF), and the CAT. This domain accommodates the relative motions of Arabia/Anatolia, Africa/Arabia and Anatolia/Africa (McKenzie 1972, 1978, Le Pichon and Angelier 1979, Sengör 1979, Jackson and McKenzie 1984, Dewey *et al.* 1986, Westaway 1994). The EAF is approximately 500 km long and runs southwestward from Karliova in eastern Anatolia (where it joins the North Anatolian Fault [NAF]) either to the Gulf of Iskenderun (Jackson and McKenzie 1984, 1988, Arger and Westaway 2000) or to the town of Antakya (Arpat and Şaroglu 1972, Perinçek and Çemen 1990, Şaroglu *et al.* 1992, Over *et al.* 2002). The NAF is a dextral strike-slip fault which runs E–W for about 1400 km, bounding the northern margin of the Anatolian block. It appears

to have been established following collision of the Eurasian and Arabian plates and with a zone of active strike-slip since the Late Pliocene. Together, sinistral motion on the EAF and dextral motion on the EAF are resulting in westward extrusion/escape of Anatolia in response to the ongoing northward drift of Arabia.

Left-lateral displacement on the EAF has been characterized by seismological observations (McKenzie 1972, Jackson and McKenzie 1984, Taymaz *et al*. 1991) and structural studies (Arpat and Şaroglu 1975, Şaroglu *et al*. 1992). According to Perinçek and Çemen (1990), Şaroglu *et al*. (1992) and Over *et al*. (2002), the major fault continuation of the EAF seems to run through the Amanos Mountains from Türkoğlu to Antakya. This interpretation of the neotectonic situation can only be part of the story because current slip on the Amanos Fault is only $\sim 1.3\,\mathrm{mm\,year^{-1}}$ (Yurtmen *et al*. 2002). Hence, the slip on the Amanos Fault is only about 10–20% of the slip on the EAF. This segment, with a NNE–SSW ($15^\circ \pm 5^\circ$) orientation is about 145 km long and is known as the Amanos (Perinçek and Çemen 1990) or Karasu Fault (Chorowicz *et al*. 1994). It bounds the western flank of the $\sim$30-km-wide Amik Basin which is now filled with Plio-Quaternary sediments (Lyberis *et al*. 1992) having a thickness of more than 1000 m (Perinçek and Eren 1990). The K-Ar, Nd, Sr and Pb isotopic dating studies have yielded a recent Quaternary age for the basaltic rocks erupted along the central part of the Karasu Valley—the bulk of the volcanic rocks which have erupted in the region (Çapan *et al*. 1987, Yürür and Chorowicz 1998, Rojay *et al*. 2001) (figure 2).

Farther south, the differential northward motion of Arabia with respect to Africa is essentially taken up by the DSF, which is approximately 1000 km long and extends northward from the Red Sea to Antakya (Nur and Ben-Avraham 1978, Lyberis *et al*. 1992). This fault is interpreted as a left-lateral intracontinental transform (Nur and Ben-Avraham 1978, Lovelock 1984, Mart and Rabinowitz 1986, Hempton 1987).

The plate boundary between southern Anatolia and the African Plate is a subduction zone comprising the Hellenic and Cyprus arcs. The deformation style along the Cyprus Arc and its extension into the Hatay region has been discussed by a number of authors. Most (McKenzie 1972, Ben-Meneham *et al*. 1976, Kempler and Garfunkel 1994, Mart and Woodside 1994) consider that the arc and its continental extension form a dominantly strike-slip fault, constituting a transform plate boundary. Thus, the Hatay region appears to experience the coeval influence of the kinematics of the major active fault zones of the eastern Mediterranean region namely the EAF, DSF and Cyprus Arc and the relative northward drift of Afro-Arabian plate as the Anatolian block moves westward.

2.2. *Seismicity and seismotectonics of the Hatay region*

The distribution of earthquakes of magnitude greater than three that occurred in Turkey between 1973 and May 2002 is given in figure 3. The earthquake data are from the United States Geological Survey (USGS). In the study area, earthquakes are mainly distributed along the CAT lineament. The 22 January 1997 Antakya earthquake, with a 5.7 seismic moment magnitude (Mw), occurred on this lineament. The lineament continues to the south of Cyprus as the Cyprus Arc. During this period, the Amanos and Dead Sea faults have been characterized by low seismicity although these are known from historical records to have been seismically active (Poirier and Taher 1980, Ambraseys and Melville 1988, Ambraseys and Barazangi 1989).

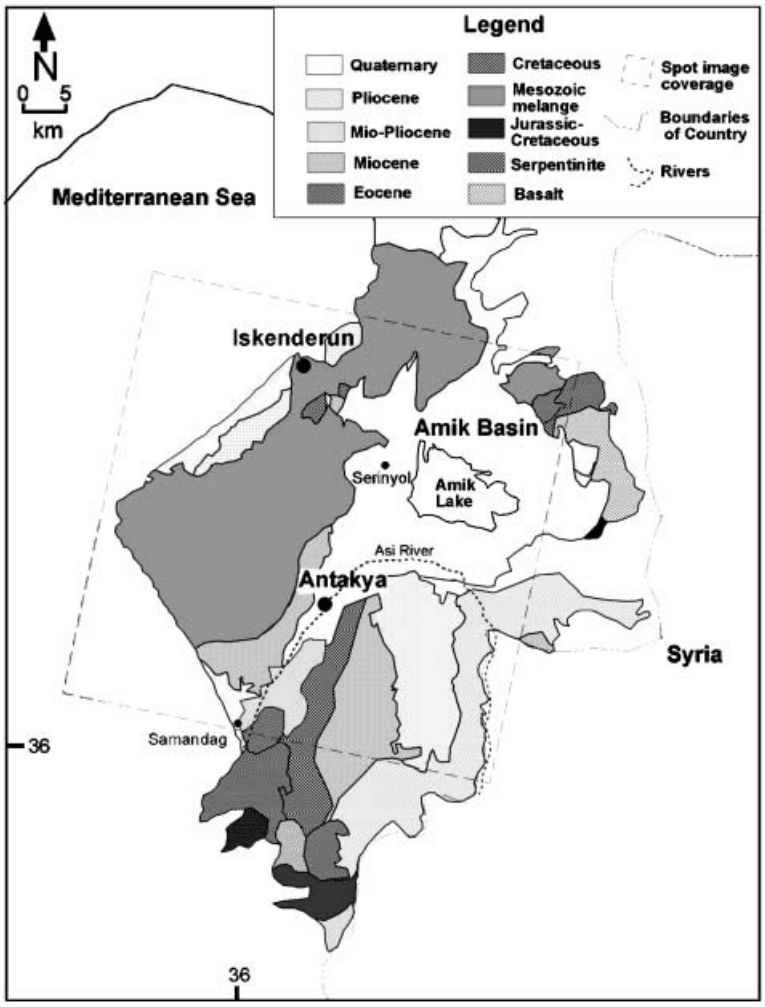


Figure 2. Simplified geological map of Hatay region (Erentöz and Pamir 1964).

The last important earthquake on 22 January 1997 was 5.5 in body-wave magnitude (mb), and aftershocks were of 5.2 and 5.3 mb magnitude. These events occurred along the NE–SW-trending CAT fault. The focal-mechanism solution of the main earthquake (using the Harward catalogues; Erdik *et al.* 1997 and Ergin 1999) yields a mean direction of NE–SW for the causative fault zone. The focal-mechanism solutions of the aftershocks confirm a NE–SW direction and show mainly a strike-slip motion along the CAT lineament. The seismicity shows that this NE–SW trending lineament is a clearly different trend from the NNE–SSW trending Amanos Fault and the roughly N–S trending DSF.

3. Lineament analysis of Hatay region with SPOT XS imagery

In this study, we used a SPOT XS image of the Hatay region that includes the Amik Basin. The region is centred on 36°21′46″ N and 36°07′46″ E and the precise geographical position of the study area is shown in figure 2.

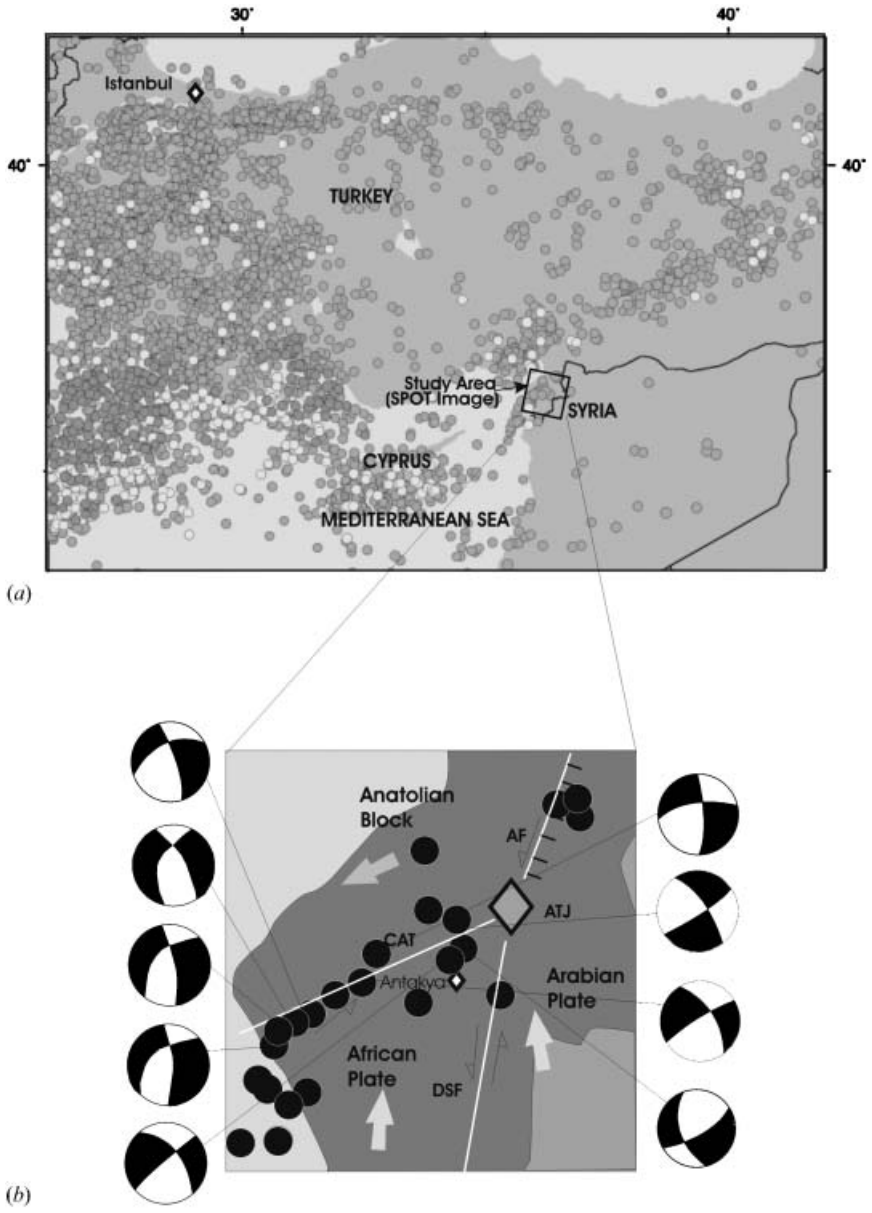


Figure 3. (*a*) Epicentre distribution of earthquakes (M > 3.0) of Turkey between 1973 and June 2002 from USGS catalogues. (*b*) Simplified seismotectonic map of study area. Arrows near the faults show the slip sense and grey arrows illustrated slip-vectors of plate motions. The focal mechanisms of earthquakes are provided by Harward CMT catalogues, Erdik *et al*. (1997) and Ergin (1999).

3.1. *Preprocessing of SPOT XS imagery*

The data set includes SPOT XS bands (K-J:118-277) as raw data (figure 4). The image was formed by 3001 pixels × 3172 pixels and was taken on 29 November 1993 with a sun elevation angle of 31° and a sun azimuth angle of 164.9°.

Before applying enhancement and the data-extraction stage, the dataset was georeferenced to the Universal Transverse Mercator (UTM) coordinate system

using ED 50 as the datum. Approximately 50 ground control points were used to correct geographically the image from the 1:25 000 scale topographic quadrangles. These points were obtained using known points (e.g. coastal features, stream crossings, road intersections) that could be easily located on the SPOT XS image. The final step was generating a 20 m UTM grid using a second-order polynomial fit with nearest-neighbour resampling technique. All preprocessing and enhancement procedures were done using the ER Mapper Version 6.2 image processing software (ER Mapper 1998). A linear contrast stretch was routinely applied to all the preprocessed and enhanced image data used in evaluation and interpretation.

SPOT XS full-scene imagery of the region covers 60 km^2. The digital SPOT XS data, which were obtained from the ISIS program (CNES), were enhanced for better geologic/tectonic interpretations. Figure 4 shows the original full study area. We subdivided the area into three sub-areas, namely Area 1, Area 2 and Area 3.

3.2. *Unsupervised classification of SPOT XS imagery*

In order to elucidate the geologic lineaments of the region, the ISODATA method of unsupervised classification was applied to the SPOT XS images that were

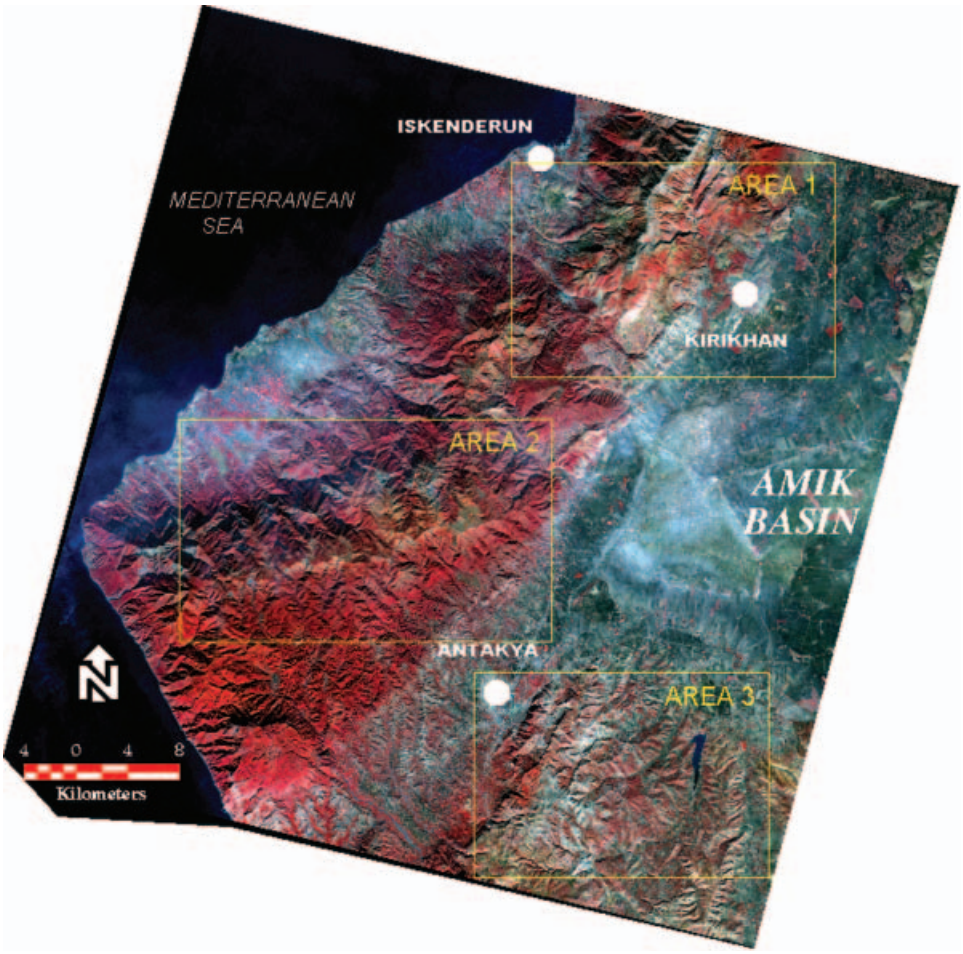


Figure 4. Spot XS imagery (K/J 118/277) covering the study area.

used in this study. This classification method is a powerful tool for deriving useful spectral information in image processing and is applied to areas from which there is little or no information (Berger 1994, Drury 2001). Thus the images were separated into approximately 15 spectral classes in the light of the geological map of the region (figure 2), and the result is given in figure 5. At a glance, mainly five notable spectral classes are observable in this figure. These are, in ascending order, rural areas in pink, topographically vast plains in magenta, agricultural areas in tones of yellow, water and shadowed areas in blue, and plant and forest cover in tones of green. The focus area in the soutwestern part of the region is the trace of CAT fault that is represented by a thin purple line. This synoptic appearance supports the possibility of a lineament system along this zone.

3.3. *Linear edge enhancement of SPOT XS imagery*

In the current study, linear edge enhancement was applied to the near infra-red band (0.79–0.89 μm) of the SPOT XS image by using an asymmetric filter with

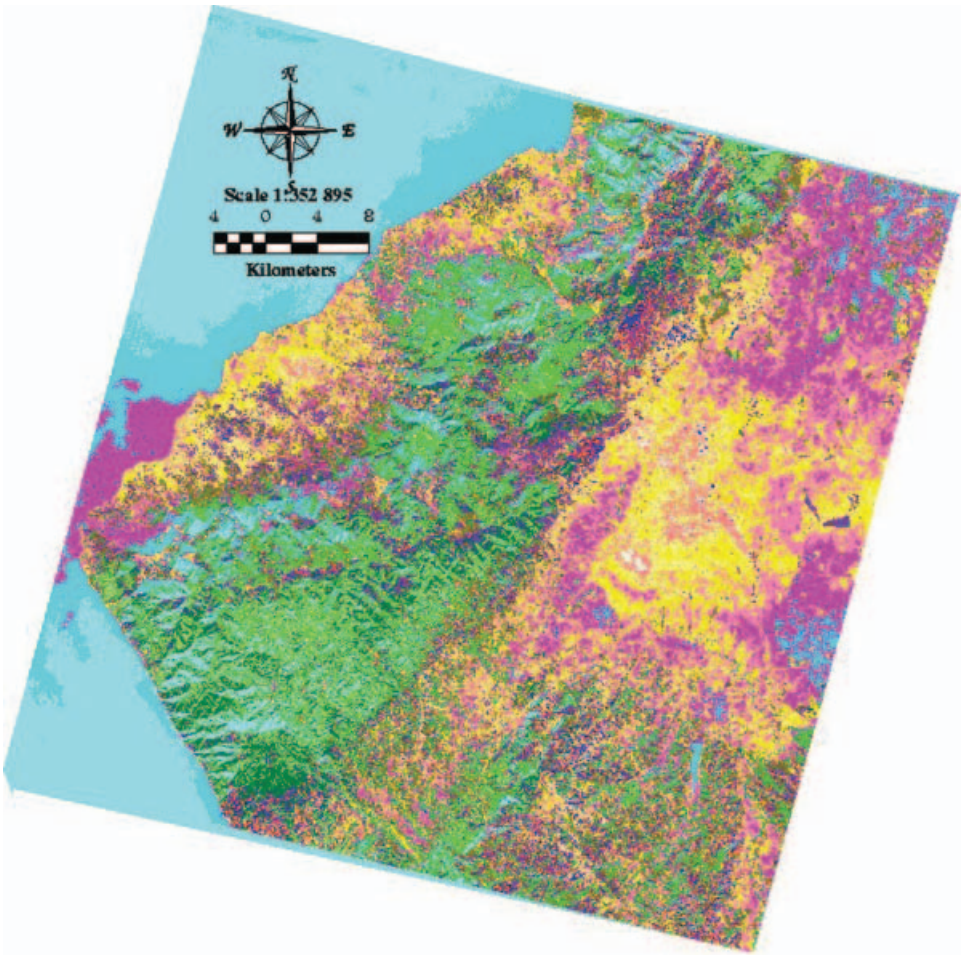


Figure 5. Appearance of spectral classes and linear feature of CAT with the aid of unsupervised classification method.

different illumination directions to highlight the dominant geological lineaments and exposure-related spatial features. The same and close spectral band coverages for structural and tectonic analysis studies both in the SPOT XS and Landsat TM digital datasets have also been used by various authors (Crósta and Moore 1989, Binelli-Chahine *et al*. 1990. Qari 1991, Yésou and Rolet 1990, Kavak and Inan 2002). With this type of filtering choice, we are able to delineate the prominent structural features within the tectonic context. We subdivided the area into three sub-areas (figure 4): Area 1 takes in the southern end of the Amanos Fault; Area 2 covers the extension of the Cyprus Arc, i.e. the CAT; and Area 3 includes the northern end of DSF (figure 4). The filter directions were chosen to expose the aforementioned lineaments. As is well known, such filters can be used to extract lineaments with preferred orientations. Linear edge or directional gradient enhancement methods are used to delineate the lineaments in a particular direction using a common rule. To reveal the geological lineaments with a particular orientation, they should be illuminated normal to their general strike directions. The total value of the kernel used for these types of studies is equal to zero, and negative values are located within it. Richards and Jia (1999) identified these filter kernels clearly, and the filters are termed Prewitt filters (Prewitt 1970). Another characteristic of these kernels is the distribution of non-zero weighting factors parallel to the direction. The authors qualified these kernels as linear edge detector templates. These 3×3 templates may be applied to an image to detect its edges in all orientations. Using these kernels, it is possible to obtain valuable results for structural applications in geology, although man-made cultural features such as transmission lines and pipelines, drainage channels, rail roads and highways should first be eliminated by visual control and interpretation. Below are shown types of kernels that were used for the second area, represented by the CAT.

1	1	0
1	0	−1
0	−1	−1

0	1	1
−1	0	1
−1	−1	0

In this study, the same filtering direction (from north-west to south-east), which aimed to extract geologic lineament systems, was applied to the southern end of the Amanos Fault (Area 1) and the northern end of DSF (Area 3), because their general trends of height are similar (figure 4). Spatial filtering used the aforementioned 3×3 template kernel. The CAT, which has a different trend, was the main focus of this study. In the same way, this part of the region was filtered using a SE–NW-trending filter to reveal lineaments in the vicinity of the on-land extension of the Cyprus Arc.

3.4. *Interpretation of lineament systems using seismicity data*

The epicentral earthquake distribution that coincides with these lineaments can support the identification of a plate boundary. Hence, the described lineaments are compared with epicentral earthquake distributions in the next section. SPOT XS image processing results show that there are three different lineaments/tectonic belts that converge east of Antakya, in the vicinity of the Quaternary Amik Basin, thus indicating the presence of a triple-junction (figure 3).

4. Study areas

Geographically, the Bay of Iskenderun forms the easternmost point of the Mediterranean Sea, northeast of Cyprus (figure 4). In Area 1 of this region, the approximate orientation of the Amanos Mountains and fault system that cross the study area is NE–SW.

The edge enhanced image in figure 6(*a*) shows Area 1 and its lineaments. The general trend of these lineaments is parallel to the southern Amanos fault system, that is NE–SW. Detailed lineament analysis of this region gave extremely valuable results over the area. Figure 6(*b*) and table 1(*a*) show a rose diagram and statistics for the area. The reason for low lineament density in the southeastern part of Area 1 is the presence of younger Amik Basin deposits that cover older units of the region over wide areas. Needless to say, different patterns of filtered images hide the significant lineaments of Area 1 (figure 6(*a*)).

A total of 90 lineaments have been observed in Area 1, and numerical values will give an analytical assessment in terms of the tectonics of the photointerpreted components of the region (table 1(*b*)). The dominant distribution anomaly of the geologic lineaments shows an indisputable predominance in the NE direction (figure 6(*b*)). The total length of these lineaments is approximately 61 km, and the densest areas are between N 40°–55° and E70–85° (table 1(*b*)). However, the maximum lineament length of the region trends approximately 90°.

The main focus area in this analysis is Area 2 and includes the CAT (Figure 7(*a*)). This zone branches mainly in three separate lineament systems that are approximately ENE–WSW-trending. Morphologically, Kızıldağ ('red mountain'), which is underlain mainly by an ophiolitic complex stretching from Serinyol to the northern part of Samandağ (figure 2), comprises the northern block of the CAT. The summit of this mountain is at roughly 1750 m even though it is located only about 30 km from the sea. The presence of such different topographic features in contiguous areas may indicate that a considerably active tectonic regime has controlled/controls the evolution of the region.

Figure 7(*a*) and table 2(*a*) present geological lineaments and their statistics for Area 2. The procedures related to lineament analysis were completed by visual analysis using topographic quadrangles and satellite data. The thin line on the rose diagram shows the mean strike of the CAT in the filtered image [(figure 7(*b*)). The length of the first component of the CAT at its westernmost point is about 5 km,

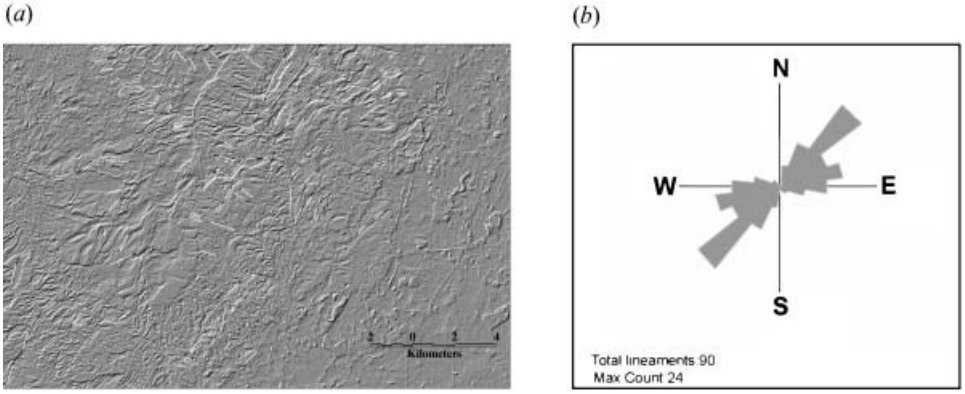


Figure 6. Lineaments derived from NW-filtering for Area 1 with the aid of directional gradient enhancement.

Table 1 (*a*) and (*b*). Statistical values of NW filtering for Area 1.

	Mid print	#Lin	Minimum length	Maximum length	Mean length	Total length	Mean angle
(*a*)	−75	6	309.44	1246.28	742.83	4456.97	−73.3
	−60	2	525.20	613.61	569.41	1138.82	−60.2
	−45	2	553.71	654.26	603.98	1207.97	−41.1
	−30	1	712.73	712.43	712.73	712.73	−28.6
	0	1	1460.79	1460.79	1460.79	1460.79	0.4
	15	5	396.00	1020.52	781.38	3906.91	16.3
	30	11	358.24	809.71	565.13	6216.48	30.9
	45	24	468.86	1131.23	705.34	16928.11	44.7
	60	12	401.83	1244.89	657.54	7890.46	59.0
	75	15	388.73	1211.02	675.63	10134.41	75.5
	90	11	16.02	1144.77	644.70	7091.68	90.3
(*b*)	All	90	16.02	1460.79	679.39	61145.31	

and it trends approximately 60°E (figure 7(*a*)). The second and third lineament segments have two different strikes, 90° and 70°, respectively. The length of the middle segment is about 7–8 km and the third is longer. As is clearly seen in table 2(*b*), the total length of the CAT and the other small lineaments reaches approximately 75 km. The lineaments between 30° and 40°, and 50° and 60° contain the densest swarms, whereas 70° and 90° have the greatest values as total length.

Area 3 generally has higher elevations than Area 2, and is bounded by the vast plains of the Amik Basin to the north and by Quaternary Asi River deposits to the west (figure 2). These topographically high areas are underlain mainly by Mio-Pliocene and Upper Cretaceous mélange units (figure 2). As is seen in figure 8(*a*), the general pattern in the northwestern part of Area 3 represents the Asi River. The area generally has densely distributed lineaments in its NW and SE parts (figure 8(*b*)). Similar to other areas, this region also has dense, NE–SW lineament orientations (figure 8(*a*) and (*b*)). The orientation N40°–50°E has the densest swarm with approximately 13 km of length (table 3(*a*)). Additionally, it contains the highest number of lineaments. This area demonstrates a tendency similar to the other areas in terms of the total number of lineaments and their lengths (table 3(*b*)).

In these types of analyses, shadowing problems related to illumination direction

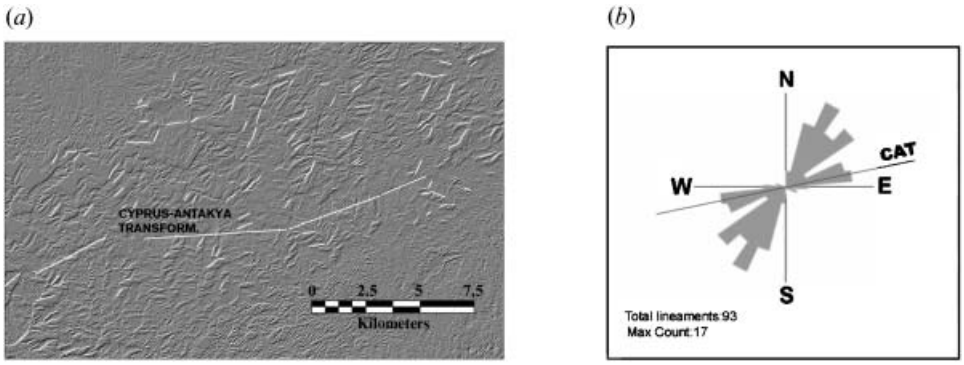


Figure 7. Lineaments derived from SE-filtering for Area 2 with the aid of directional gradient enhancement.

Table 2 (*a*) and (*b*). Statistical values of SE filtering for Area 2.

	Mid point	#Lin	Minimum length	Maximum length	Mean length	Total length	Mean angle
(*a*)	−80	1	702.59	702.59	702.59	702.59	−75.7
	−70	2	379.93	832.92	606.42	1212.85	−70.0
	10	3	443.75	892.44	600.62	1801.86	11.3
	20	12	401.59	1083.36	602.22	7226.58	21.6
	30	17	347.99	1034.90	565.29	9609.93	30.8
	40	12	398.25	966.49	658.22	7898.67	40.5
	50	15	344.51	750.54	530.13	7951.98	50.5
	60	4	373.53	4667.78	1557.37	6229.49	61.3
	70	11	307.83	5586.13	1347.64	14824.03	69.3
	80	12	415.76	904.31	657.04	7884.50	80.3
	90	4	307.33	8327.47	2429.39	9717.55	86.7
(*b*)	All	93	307.33	8327.47	807.10	75060.02	

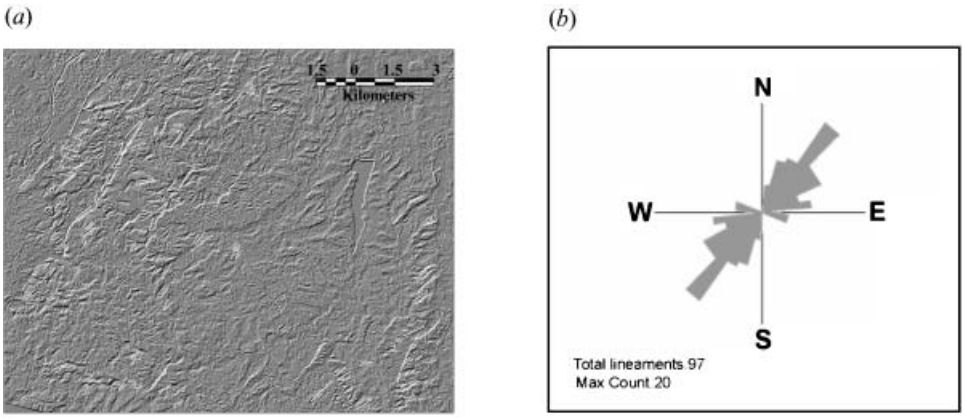


Figure 8. Lineaments derived from NW-filtering for Area 3 with the aid of directional gradient enhancement.

Table 3 (*a*) and (*b*). Statistical values of NW filtering for Area 3.

	Mid point	#Lin	Minimum length	Maximum length	Mean length	Total length	Mean angle
(*a*)	−80	5	371.77	623.77	499.32	2496.60	−79.0
	−70	5	259.33	684.79	523.56	2617.78	−71.2
	10	5	395.43	584.13	485.64	2428.18	11.5
	20	10	373.02	1980.41	856.63	8566.30	23.1
	30	11	264.88	1362.53	779.95	8579.40	30.4
	40	20	270.98	1356.58	647.46	12949.22	39.3
	50	12	407.27	1631.81	821.42	9857.08	50.7
	60	12	0.05	890.38	574.57	6894.79	59.0
	70	7	244.54	1065.37	588.81	4121.64	69.1
	80	9	426.33	2229.36	931.31	8381.79	79.2
	90	1	914.02	914.02	914.02	914.02	87.2
(*b*)	All	97	0.05	2229.36	699.04	67806.79	

may cause the interpreter to produce misleading results because of the non-illuminated sides of topographic highs. The elongated peaks of sharp hills may produce some patterns that appear similar to geological lineaments. In addition, if the units cropping out in a region are made up of resistant rocks, these may also produce oriented ridges which resemble geological lineaments. To avoid such types of mistakes, the interpreter should eliminate false linear features with the aid of visual interpretation. Sun azimuth and elevation angles at the time of acquisition of satellite imagery and the choice of filtering direction are the determinative factors for lineament analysis studies. On the other hand, if the direction of the edge enhancement filter is not affected by opposing geomorphologic features, it may indicate proper lineament distribution. In this study, geologic lineaments derived from filtered imagery were carefully drawn on an overlay, keeping in mind the aforementioned considerations. The resultant images with lineaments are shown in figures 6(*a*), 7(*a*) and 8(*a*).

5. The Antakya triple junction

The deformations that have been observed near the joint of the Arabian, African and Eurasian continental plates are largely controlled by the northward convergent motion of Africa and Arabia relative to Anatolia. Regional studies dealing with the tectonics of the Middle East and the eastern Anatolian region have yielded several different interpretations for the structural relationship between the two (EAF and DSF) sinistral strike-slip faults. Several authors claim that the EAF disappears to the south of Kahramanmaraş (McKenzie 1972, Muehlberger and Gorbon 1987) and state that the relationship between the EAF and DSF is unclear. Some workers suggest a triple junction at the termination of the EAF, inferred to be near Türkoğlu (Gülen *et al.* 1987, Lyberis *et al.* 1992). In contrast, other researchers claim that the EAF changes strike to the south of Kahramanmaraş and that the trace passes through the Hatay region to the city of Antakya, where it meets the DSF (Arpat and Şaroğlu 1975, Perinçek and Çemen 1990, Şaroğlu *et al.* 1992, Over *et al.* 2002). Based on a field study using structural observations, Perinçek and Çemen (1990) noted triple junction points at three different localities: at Antakya, near Türkoğlu (Kahramanmaraş), and farther northeast near Hazar Lake. Their Antakya triple junction was defined by two boundary faults, namely the Amanos Fault as part of the EAF and the DSF. However, they did not define their third boundary belt. Şaroğlu *et al.* (1992) defined a triple junction in the vicinity of Antakya between the EAF and DSF plate boundaries and a small NNW–SSE-trending dextral local segment, named the Reyhanlı Fault, which evidently does not represent any plate, sub-plate or block boundary. Yürür and Chorowicz (1998), on the basis of field structural data, interpreted the triple junction near Türkoğlu (MTJ) to have formed in the Middle Miocene after which it moved to the vicinity of Antakya $\sim$2 Ma. Their triple junction is defined by the Amanos Fault, the DSF and the SW continuation of the EAF to the south of Cyprus. Their third segment corresponds to the CAT observed in this study. In their model, the continuation of the EAF does not define the boundary although in our interpretation, the CAT lineament, which continues to the Cyprus Arc, is defined as a boundary between the African Plate and the Anatolian block, considered to be a part of the Eurasian plate.

Thus, previous investigations and our observations based on SPOT XS imagery and seismotectonic features show that three major belts (i.e. the Amanos Fault, DSF and CAT) are close to each other in southern Anatolia, particularly in the vicinity of the city of Antakya, and form a triple junction. The definition of these

lineaments suggests that the triple junction could be located over quite a large area in the vicinity of Antakya. However, the Quaternary Amik Basin is the obvious tectonic feature close to this intersection of the Amanos Fault (considered here as the southern part of EAF), the DSF strike-slip fault zone (Perinçek and Çemen 1990, Lyberis *et al*. 1992) and the CAT lineament.

The Antakya triple junction (ATJ) is schematically illustrated in figure 9. The Amanos Fault, as the southern part of left-lateral strike-slip EAF, has been accommodated by transtension with a SW-extensional direction operative during the Quaternary (Over *et al*. 2002). This fault is assumed to be the boundary between Arabia and Anatolia. The left-lateral strike-slip DSF, representing the plate boundary between Arabia and Africa, seems to die out in the vicinity of Antakya (Lyberis *et al*. 1992). The CAT, the focus of this study, is clearly revealed by both the SPOT XS imagery and seismotectonic analysis. The majority of focal-mechanism solutions were made by Erdik *et al*. (1997) and Ergin (1999) and give a left-lateral strike-slip solution with a normal component along the CAT lineament.

6. Conclusion

High-pass spatial filtering has always been a good choice for geological applications, particularly in structural studies (Binelli-Chahine *et al*. 1990, Yésou and Rolet 1990). SPOT XS image attributes have more spatial advantages in comparison to other remote-sensing systems (Chavez and Bowell 1988). From the results of the filtering process and the unsupervised classification method used here, it can be seen that geological lineament analysis has been successful in the study area, particularly in defining the CAT with its NE–SW trend. Results of the detailed visual and statistical lineament analysis and classification method are compatible with

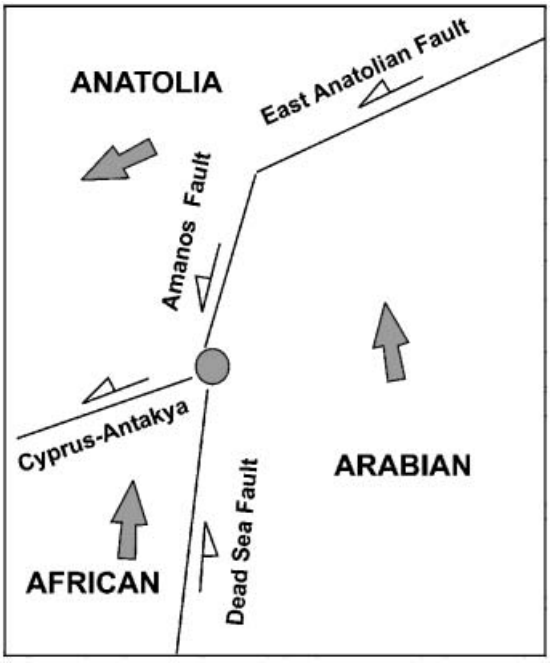


Figure 9. Tectonic evolution of the study area is showing formation of Antakya Triple-Junction (ATJ). Grey arrows indicate slip-vectors of plate motions.

each other in terms of the trends of these lineament systems and their total lengths. Individual lengths ($\sim$70 km) for the three different areas were numerically similar to one another. The oriented NE trends of the lineaments in rose diagrams provide clear evidence for the presence of the CAT and the other systems.

According to this point of view, the tectonic lineaments recognised in this study permit us to clearly identify the NE–SW trend of the Cyprus–Antakya zone as a transform lineament. From seismotectonic analysis, fracture measurements in the field (Over *et al*. 2002), and SPOT XS imagery analysis, this NE–SW-trending trace (Area 2) is interpreted as a tectonic lineament which seems to continue to the south of Cyprus, there connecting with the Cyprus Arc. It dies out in the Quaternary Amik Basin which appears to have been formed by the intersections of three tectonic lineaments, namely the Amanos Fault (Area 1) forming the southern part of the EAF, the northern part of the DSF (Area 3), and the CAT lineament (Area 2), with the latter as the on-land extension of the Cyprus Arc. This triple junction, located among Arabia, Africa and Anatolia, is comparable to the theoretical transform–transform–transform (FFF) type defined by McKenzie and Morgan (1969), and should be in unstable position. On the other hand, Over *et al*. (2002) suggested that a roll-back process between Africa and Anatolia along the Cyprus Arc has contributed to the SW-directed extensional movement of the whole region in the Quaternary. For this reason, the former position of the triple junction should have shifted toward the SW. Thus, both the roll-back process and the triple junction system have played important roles in the evolution of the basin since Quaternary time. Perhaps the centre of the basin was the former location of the actual triple junction area earlier in the Quaternary.

These major faults, which are proximal to each other in the vicinity of the Amik Basin, form a triple junction (Antakya triple junction) to accommodate deformation between Arabia/Anatolia, Africa/Arabia and Anatolia/Africa.

Acknowledgments

This work was financially supported by the Research Foundation of Cumhuriyet University (Project No. M 121). The authors thank the ISIS program (CNES) for providing SPOT data. Special thanks are due to Dr John D.A. Piper (Liverpool University) and Dr Steve Mittwede (English editor of *Turkish Journal of Earth Sciences*/TUBITAK) for complete revision of the English manuscript. We are also grateful to the anonymous reviewers for their valuable comments and suggestions that greatly improved the quality of our manuscript.

References

AMBRASEYS, N. N., and BARAZANGI, M., 1989, The 1759 earthquake in the Bekaa Valley: implications for earthquake hazard assessment in the eastern Mediterranean region. *Journal of Geophysical Research*, **94**, 4007–4013.

AMBRASEYS, N. N., and MELVILLE, C. P., 1988, An analysis of the eastern Mediterranean earthquake of 20 May 1202. In *Historical Seismograms and Earthquakes of the World*, edited by W. H. K. Lee, H. Meyers and K. Shimazaki (San Diego: Academic), pp. 181–200.

ARPAT, E., and ŞAROĞLU, F., 1972, The East Anatolian fault system: thoughts on its development. *Bulletin of Mineral Research and Exploration of Turkey*, **78**, 33–39.

ARPAT, E., and ŞAROGLU, F., 1975, Some recent tectonic events in Turkey. *Bulletin of Geological Society of Turkey*, **18**, 91–101.

BEN-MENEHAM, A., NUR, A., and VERED, M., 1976, Tectonic seismicity and structure of the Afro-Eurasian junction, the breaking of an incoherent plate. *Physical Earth Planet Inter*, **12**, 1–50.

BERGER, Z., 1994, *Satellite Hydrocarbon Exploration, Interpretation and Integration Techniques* (New York: Springer-Verlag).

BINELLI-CHAHINE, M., VERGELY, P., and MASON, P., 1990, Computer processing of Landsat and SPOT images for the morpho-structural analysis of the Wei He Graben (Shaanxi-China). Preliminary results. *ISPRS International Journal of Photogrammetry and Remote Sensing*, **45**, 297–315.

CRÓSTA, A. P., and MOORE, J. MC. M., 1989, Geologic mapping using Landsat Mapper imagery in Almeria province, South-East Spain. *International Journal of Remote Sensing*, **10**, 505–514.

CHAVEZ, P. S. JR, and BOWELL, J. A., 1988, Comparison of the spectral information content of Landsat Thematic Mapper and SPOT for three different sites in the Phoenix, Arizona region. *Photogrammetric Engineering and Remote Sensing*, **54**, 1699–1708.

CHOROWICZ, J., LUXEY, P., LYBÉRIS, N., CARVALHO, J., PARROT, J. F., YÜRÜR, T., and GÜNDOĞDU, N., 1994, The Maraş Triple Junction (southern Turkey) based on digital elevation model and satellite imagery interpretation. *Journal of Geophysical Research*, **99**, 20225–20242.

ÇAPAN, U. Z., VIDAL, P., and CANTAGREL, J. M., 1987, K-Ar, Nd, Sr and Pb isotopic study of the Quaternary volcanism in Karasu Valley (Hatay), N-end of Dead Sea rift zone in SE Turkey. *Bulletin of Earth Science, Hacetepe University, Ankara*, **14**, 165–178.

DEWEY, J. F., HEMPTON, M. R., KIDD, W. S. F., SAROGLU, F., and SENGÖR, A. M. C., 1986, Shortening of continental lithosphere: the neotectonics of Eastern Anatolia—a young collision zone. In *Collision Tectonics*, edited by M. P. Coward and A. C. Ries (London: Geological Society), Special Publication, **19,** 3–36.

DRURY, S. A., 2001, *Image Interpretation in Geology*, 3rd edition (Oxford: Blackwell Science).

ERDİK, M., AYDINOĞLU, N., PINAR, A., and KALAFAT, D., 1997, Report of Hatay Earthquake, Kandilli Obs, Istanbul.

ERENTÖZ, C., and PAMIR, H. N., 1964, *1:500 000 Geological Map of Turkey* (Ankara: MTA).

ERGİN, M., 1999, Present day seismicity and seismotectonic characteristics of the Cilician region, PhD Thesis, Istanbul Technical University.

ER MAPPER, 1998, Tutorial.

GÜLEN, L., BARKA, A. A., and TOKSÖZ, M. N., 1987, Kıtaların çarpışması ve ilgili komplex deformasyon: Maraş üçlü eklemi ve çevre yapıları. *Bulletin of Earth Science, Hacetepe University, Ankara*, **14**, 319–336.

GÜRSOY, H., PIPER, J. D. A., TATAR, O., and MESCİ, L., 1998, Paleomagnetic study of the Karaman and Karapınar volcanic complex, central Turkey: neotectonic rotation in the south central sector of the Anatolian Block. *Tectonophysics*, **299**, 191–211.

HEMPTON, M. R., 1987, Constraints on Arabian plate motions; an extensional history of the Red sea. *Tectonics*, **6**, 668–705.

JACKSON, J., and MCKENZIE, D. P., 1984, Active tectonics of the Alpine–Himalayan belt between western Turkey and Pakistan. *Geophysical Journal of the Royal Astronomical Society*, **C77**, 185–264.

JACKSON, J., and MCKENZIE, D. P., 1988, The relationship between plate motion and seismic moment tensors, and the rates of active deformation in the Mediterranean and Middle East. *Geophysical Journal of the Royal Astronomical Society*, **93**, 45–73.

KAVAK, K. S., and İNAN, S., 2002, Enhancement facilities of SPOT XS imagery in remote sensing geology: an example from the Sivas Tertiary Basin (Central Anatolia/ Turkey). *International Journal of Remote Sensing*, **23**, 701–710.

KEMPLER, D., and GARFUNKEL, Z., 1994, Structures and kinematics in the northeastern Mediterranean: a study of an irregular plate boundary. *Tectonophysics*, **234**, 19–32.

LE PICHON, X., and ANGELIER, J., 1979, The Hellenic arc and trench system: a key to the neotectonic evolution of the eastern Mediterranean area. *Tectonophysics*, **60**, 1–42.

LOVELOCK, P. E. R., 1984, A review of the tectonics of the northern Middle-East region. *Geological Magazine*, **121**, 577–587.

LYBERIS, N., YURUR, T., CHOROWICZ, J., KASAPOGLU, E., and GÜNDOGDU, N., 1992, The East Anatolian Fault: an oblique collisional belt. *Tectonophysics*, **204**, 1–15.

MART, Y., and WOODSIDE, J., 1994, Preface: tectonics of the Eastern Mediterranean. *Tectonophysics*, **234**, 1–3.

MART, Y., and ROBINOWITZ, P. D., 1986, The northern Red Sea and the Dead Sea rift. *Tectonophysics*, **124**, 85–113.

McKENZIE, D. P., 1972, Active tectonics of the Mediterranean Region. *Geophysical Journal of the Royal Astronomical Society*, **30**, 109–185.

McKENZIE, D. P., 1978, Active tectonics of the Alpine–Himalayan belt: the Aegean sea and surrounding regions (tectonic of Aegean region). *Geophysical Journal of the Royal Astronomical Society*, **55**, 217–254.

McKENZIE, D. P., and MORGAN, W. J., 1969, Evolution of triple junctions. *Nature*, **224**, 125–133.

MUEHLBERGER, W. B., and GORBON, M. B., 1987, Observations on the complexity of the East Anatolian Fault, Turkey. *Journal of Structural Geology*, **9**, 899–903.

NUR, A., and BEN-AVRAHAM, Z., 1978, The eastern Mediterranean and the Levant: tectonics of continental collision. *Tectonics*, **46**, 297–311.

OVER, S., ÜNLÜGENÇ, U. C., and BELLIER, O., 2002, Quaternary stress regime change in the Hatay region (SE Turkey). *Geophysical Journal International*, **148**, 1–14.

PERİNÇEK, D., and ÇEMEN, I., 1990, The structural relationship between the East Anatolian Fault and Dead Sea Fault zones in southern Turkey. *Tectonophysics*, **172**, 331–340.

PERİNÇEK, D., and EREN, A. G., 1990, Doğrultu atımlı Doğu Anadolu ve Ölü Deniz fay zonları etki alanında gelişen Amik havzasının kökeni. *Proceedings of 8th Oil Congress of Turkey*, 180–192.

POIRIER, J. P., and TAHER, M. A., 1980, Historical seismicity in the Near and Middle East, North Africa and Spain from Arabic documents. *Bulletin of the Seismological Society of America*, **70**, 2185–2201.

PREWITT, J. M. S., 1970, Object enhancement and extraction. *Picture Processing and Psycopictoris,* edited by B. S. Lipkin and A. Rosenfeld (New York: Academic Press), pp. 75–149.

QARI, M. Y. H. T., 1991, Application of Landsat TM data to geological studies, Al-Khabt area, southern Arabian shield. *Photogrammetric Engineering and Remote Sensing*, **57**, 421–429.

RICHARDS, J. A., and JIA, X., 1999, *Remote Sensing Digital Image Analysis* (New York: Springer-Verlag).

ROJAY, B., HEIMANN, A., and TOPRAK, V., 2001, Neotectonic and volcanic characteristics of the Karasu Fault zone (Anatolia, Turkey): the transition zone between the Dead Sea transform and the East Anatolian fault zone. *Geodinamica Acta*, **14**, 197–212.

ŞAROĞLU, F., EMRE, Ö., and KUŞÇU, I., 1992, The East Anatolian fault zone of Turkey. *Annales Tectonicae*, **VI**, 99–125.

ŞENGÖR, A. M. C., 1979, The North Anatolian transform fault: its age, offset and tectonic significance. *Journal of the Geological Society of London*, **136**, 269–282.

ŞENGÖR, A. M. C., GÖRÜR, N., and ŞAROGLU, F., 1985, Strike-slip faulting and related basin formation in zones of tectonic escape: Turkey as a case study. In *Strike-slip Deformation, Basin Formation and Sedimentation,* edited by K. T. Biddle and N. Christie-Blick (Tulsa: Society of Economics Paleontology and Minerals), *Special Publication,* **37**, pp. 227–264.

TAYMAZ, T., EYIDOĞAN, H., and JACKSON, J., 1991, Source parameters of large earthquakes in the East Anatolian Fault Zone (Turkey). *Geophysical Journal International*, **106**, 537–550.

WESTAWAY, R., 1994, Present-day kinematics of the Middle East and eastern Mediterranean. *Journal of Geophysical Research*, **99**, 12071–12090.

WESTAWAY, R., and ARGER, J., 1996, The Gölbaşı basin, southeastern Turkey: a complex discontinuity in a major strike-slip fault zone. *Journal of the Geological Society, London*, **153**, 729–744.

YÜRÜR, T., and CHOROWICZ, J., 1998, Recent volcanism, tectonics and plate kinematics near the junction of African, Arabian and Anatolian plates in the eastern Mediterranean. *Journal of Volcanology and Geothermal Research*, **85**, 1–15.

YÉSOU, H., and ROLET, J., 1990, Regional mapping of the South Armorican shear zone (Brittany, France) using remotely sensed SPOT imagery. *ISPRS International Journal of Photogrammetry and Remote Sensing*, **45**, 419–427.

YURTMEN, S., GUILLOU, H., WESTAWAY, R., ROWBOTHAM, G., and TATAR, O., 2002, Rate of strike-slip motion on the Amanos Fault (Karasu Valley, southern Turkey) constrained by K–Ar dating and geochemical analysis of Quaternary basalts. *Tectonophysics*, **344**, 207–246.